Available online at www.sciencedirect.com
SCIENCE DIRECT
Polymer 46 (2005) 9461–9475
polymer
www.elsevier.com/locate/polymer

From stiff plastic to elastic polypropylene: Polymorphic transformations during plastic deformation of metallocene-made isotactic polypropylene

Claudio De Rosa[a,*], Finizia Auriemma[a], Giordano De Lucia[a], Luigi Resconi[b]

[a]*Dipartimento di Chimica, Università di Napoli 'Federico II', Complesso Monte S. Angelo, Via Cintia, 80126 Napoli, Italy*
[b]*Basell Polyolefins, Centro Ricerche G. Natta, P.le G. Donegani 12, I-44100 Ferrara, Italy*

Received 21 April 2005; received in revised form 1 July 2005; accepted 8 July 2005
Available online 11 August 2005

Abstract

An analysis of the mechanical properties and polymorphic transformations occurring during plastic deformation of isotactic polypropylene with variable stereoregularity, containing only *rr* stereo-defects, is presented. Thermoplastic materials showing high stiffness, or high flexibility, or elastic properties can be produced depending on the concentration of defects. Relationships between the different mechanical behavior and the different observed polymorphic transformations occurring during tensile deformation are discussed. The elastic behavior of the poorly isotactic samples and the values of the corresponding mechanical parameters are related to the structural transformations occurring during stretching. The γ-form present in the unstretched sample transforms by stretching into the α-form, which in turn, transforms into the mesomorphic form at very high deformations. The mesomorphic form transforms back into the crystalline α-form upon releasing the tension and elastic recovery is observed. The crystallization of the mesomorphic form into the α-form upon releasing the tension is not observed in the case of flexible or stiff-plastic samples, which do not show elastic behavior. This indicates that in the elastomeric samples elasticity is probably partially due to the enthalpic contribution associated with the crystallization of the mesomorphic form into the α-form.

Keywords: Isotactic polypropylene; Structure–properties relationships; Polymorphic transitions

1. Introduction

The development of metallocene catalysts for the polymerization of olefins has allowed production of new materials having microstructures that cannot be obtained with conventional Ziegler–Natta catalysts [1–4]. In the case of polypropylene, any type and degree of stereoregularity, from highly isotactic to highly syndiotactic, can be produced [4]. The fine-tuning of the microstructure is nowadays possible through the rational choice of the catalytic system, and polypropylenes characterized by different kinds and amounts of regio- and stereo-irregularities, different distributions of defects and different molecular masses, are now available [4].

Recent studies of the crystallization properties of metallocene-made polypropylene have demonstrated that the microstructure strongly influences the crystal structure, the polymorphic behavior and, as a consequence, the physical properties of isotactic polypropylene (i-PP) [5–13]. Depending on type and concentration of microstructural defects, and their distribution along the polymer chain, polypropylenes with different melting temperatures having physical properties of stiff thermoplastic materials or of elastomers, can be obtained [13].

In particular polypropylenes of very high isotacticities (*mmmm* ≥ 99%) and molecular weights and melting points as high as 160 °C [14], or less stereoregular, but fully regioregular polypropylenes, are produced with a variety of C_2-symmetric complexes [15,16].

Elastomeric polypropylene has instead been obtained with different classes of metallocene catalysts. For instance, poorly isotactic polypropylene with low melting temperatures, or amorphous polypropylene, showing elastic properties has been produced by different C_1-symmetric

* Corresponding author. Tel.: +39 81 674346; fax: +39 81 674090.
E-mail addresses: claudio.derosa@unina.it (C. De Rosa), derosa@chemistry.unina.it (C. De Rosa).

0032-3861/$ - see front matter © 2005 Elsevier Ltd. All rights reserved.
doi:10.1016/j.polymer.2005.07.028

metallocene catalysts described by Chien [17], Collins [18] and Rieger [19], or by C_{2v}-symmetric and C_2-symmetric *ansa*-zirconocene complexes described by Resconi et al. [20–24]. Moreover, elastomeric polypropylene has been also produced with unbridged oscillating zirconocene catalysts, described by Coates and Waymouth [25], which produce a reactor blend of stereoblock polypropylene with different tacticities and melting temperatures. In most of these cases the elastic properties arises from the crystallization of poorly isotactic sequences [12,13,17–19,23] or of stereoblocks [9,11,25].

Depending on the used catalysts and the corresponding polymerization mechanism, different types of microstructural defects may be present in the polypropylene macromolecules (defects of stereoregularity as for instance isolated *rr* triad, and/or defects of regioregularity as for instance secondary 2,1 insertions of monomer in a prevailing primary 1,2 enchainment). The different produced microstructures induce a different crystallization behavior (in particular crystallization of α- or γ-forms is observed) [5–13,26–29] and different physical properties [12,13].

A unified view of the crystallization behavior of metallocene-made polypropylene has been recently suggested [10,12,13]. i-PP samples characterized by chains including different types of microstructural defects (strereodefects and regiodefects) generated by different catalysts, generally crystallize as a mixture of α- and γ-forms [5–13]. The fraction of γ-forms increases with increasing crystallization temperature and the content of defects [5–13,28,29]. Since the defects are randomly distributes along the polymer chains even a small amount of defects shortens the length of the regular isotactic sequences, reducing the melting temperature and favoring the crystallization of the γ-form [9–13]. Crystals of the γ-form obtained in these samples always present structural disorder [8,10,12,13], characterized a succession of bilayers of chains along a crystallographic direction with chain axes either parallel, as in the α-form, or perpendicular to each other, as in the γ-form [8]. Therefore, metallocene made i-PP crystallize in a continuum of disordered modifications intermediate between α- and γ-forms, the amount of disorder being dependent on the crystallization conditions and on the stereoregularity of the sample [8,10].

In this paper we report a study of the mechanical properties of metallocene-made i-PP samples containing only one kind of stereo-irregularity (isolated *rr* triads) in a wide range of concentration. The relationships between content of *rr* defects and mechanical properties are analyzed and related to the crystallization behavior and polymorphic transitions occurring during the plastic deformation.

2. Experimental section

i-PP samples have been prepared with the zirconocene catalysts shown in Chart 1 activated with methylalumoxane (MAO) [15,16,30–33]. All propylene polymerizations have been performed in liquid propylene at polymerization temperatures between 30 and 70 °C. Some of the MAO-activated complexes were also supported on porous polyethylene and polypropylene spheres by following a Basell technology [34] and tested under the same non-supported system. All the analyzed samples are listed in Table 1. The more isotactic sample iPP1 has been prepared with the C_2-symmetric catalyst **1**, *rac*-H_2C(3-*t*butyl-indenyl)$_2ZrCl_2$ [15,16]. The samples iPP2–iPP7 have been prepared with the C_1-symmetric *ansa*-zirconocenes **2–7** of Chart 1, based on the (substituted indenyl)-dimethylsilyl-[bis(2-methylthieno)cyclopentadienyl] ligand framework [30–33]. These catalysts are highly active in propylene polymerization and produce highly regioregular, high molecular weight i-PPs characterized by different stereoregularity and containing only *rr* triad stereodefects.

The intrinsic viscosity [η] was measured in tetrahydronaphtalene at 135 °C using standard Ubbelohde viscosimeter. The average molecular masses of i-PP samples were obtained from their intrinsic viscosity values according to $[\eta] = K(\bar{M}_v)^{\alpha}$, with $K = 1.93 \times 10^{-4}$ and $\alpha = 0.74$ [35].

The GPC curves of the samples show narrow molecular mass distributions, typical of single-center zirconocene catalysts, with polydispersity indices M_w/M_n variable in the range 2–3.

The melting temperatures were obtained with a differential scanning calorimeter Perkin–Elmer DSC-7 performing scans in a flowing N_2 atmosphere and heating rate of 10 °C/min.

Oriented fibers of the i-PP samples have been obtained by stretching at room temperature and at drawing rate of 10 mm/min compression molded samples. Compression-molded samples have been prepared by heating powder samples at temperatures higher than the melting temperatures under a press at low pressure, and slowly cooling to room temperature.

X-ray diffraction patterns were obtained with Ni filtered Cu K_α radiation. The powder profiles were obtained with an automatic Philips diffractometer, whereas the fiber diffraction patterns were recorded on a BAS-MS imaging plate (FUJIFILM) using a cylindrical camera and processed with a digital imaging reader (FUJIBAS 1800). The X-ray fiber diffraction patterns have been recorded for stretched fibers soon after the stretching and keeping the fiber under tension, as well as for relaxed fibers, that is, after keeping the fiber under tension for 2 h and then removing the tension allowing the complete relaxation of the specimens.

The index of crystallinity was evaluated from the X-ray powder diffraction profiles by the ratio of the crystalline diffraction area and the total area of the diffraction profile. The amorphous halo has been obtained from the X-ray diffraction profile of an atactic polypropylene, then it was scaled and subtracted to the X-ray diffraction profiles of the semicrystalline samples.

The relative amount of crystals in the γ-form present in our samples was measured from the X-ray powder

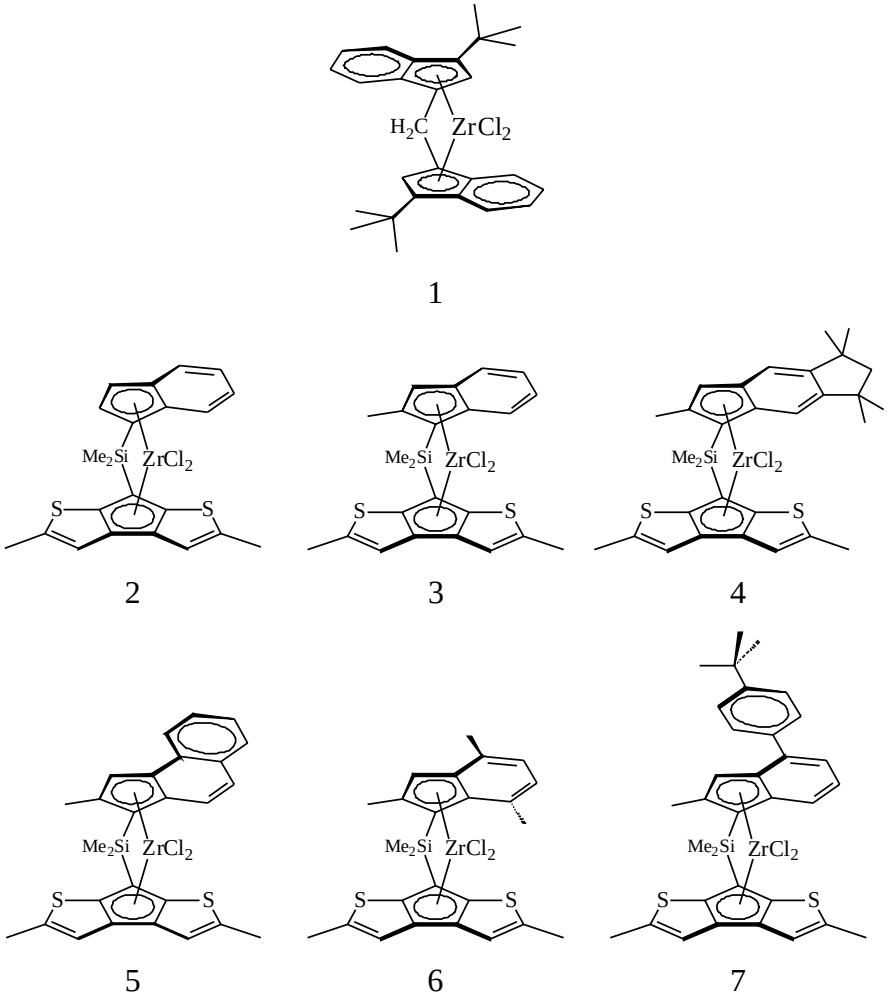

Chart 1. Structures of C_2-symmetric (**1**) and C_1-symmetric zirconocene (**2**–**7**) pre-catalysts.

diffraction profiles, by measuring the ratio between the intensities of the $(117)_\gamma$ reflection at $2\theta = 20.1°$, typical of the γ-form, and the $(130)_\alpha$ reflection at $2\theta = 18.6°$, typical of the α-form: $f_\gamma = I(117)_\gamma/[I(130)_\alpha + I(117)_\gamma]$. The intensities of $(117)_\gamma$ and $(130)_\alpha$ reflections were measured from the area of the corresponding diffraction peaks above the diffuse background intensity in the X-ray powder diffraction profiles.

Mechanical tests have been performed at room temperature on compression-molded films and oriented fibers with a miniature mechanical tester apparatus (Minimat, by Rheometrics Scientific), following the standard test method for tensile properties of thin plastic sheeting ASTM D882-83. Compression-molded films have been prepared by heating powder samples at temperatures higher than the melting temperatures between perfectly flat brass plates under a press at very low pressure, and slowly cooling to room temperature. Special care has been taken to obtain films with uniform thickness (0.3 mm) and minimize surface roughness, according to the recommendation of the standard ASTM D-2292-85.

Mechanical tests have been first performed on the unstretched compression-molded films. Rectangular specimens 10 mm long, 5 mm wide and 0.3 mm thick have been stretched up to the break or up to a given deformation $\varepsilon = [(L_f - L_0)/L_0] \times 100$, where L_0 and L_f are the initial and final lengths of the specimen, respectively. Two bench marks have been placed on the test specimens and used to measure elongation. Similar tests have been then performed at room temperature on the strained and then stress-relaxed fibers. Stress-relaxed fiber specimens have been prepared by stretching the compression molded films of initial length L_0 up to strains of 500 and 1000% (final lengths $L_f = 6L_0$ and $11L_0$), keeping the fibers under tension for 10 min at room temperature, then removing the tension, allowing the specimens to relax to the final length L_r.

Values of tension set and elastic recovery were measured according to the standard test method ASTM D412-87. The specimens of initial length L_0 were stretched up to a length L_f, i.e. up to the deformation $\varepsilon = [(L_f - L_0)/L_0] \times 100$, and held at this elongation for 10 min, then the tension was removed, and the final length of the relaxed specimens L_r

Table 1
Polymerization temperatures (T_p), viscosity average molecular masses (M_v), melting temperatures (T_m), and content of triads and pentads stereosequences (%) of i-PP samples prepared with catalysts of Chart 1

Sample	Catalyst/cocatalyst/carrier[a]	T_p (°C)	M_v[b]	T_m[c] (°C)	*mm* (%)	*mr* (%)	*rr* (%)	*mmmm* (%)	*mmmr* (%)	*rmmr* (%)	*mmrr* (%)	*xmrx* (%)	*rmrm* (%)	*rrrr* (%)	*rrrm* (%)	*mrrm* (%)
iPP1	**1**/MAO	50	195,700	162	98.52	0.99	0.49	97.55	0.97	0.00	0.97	0.01	0.00	0.00	0.00	0.49
iPP2	**7**/MAO/PE	60	106,000	140	92.37	5.08	2.54	87.61	4.70	0.06	4.70	0.26	0.13	0.06	0.13	2.35
iPP3	**6**/MAO/PP	60	202,400	133	88.90	7.40	3.70	82.19	6.58	0.14	6.58	0.55	0.27	0.14	0.27	3.29
iPP4	**3**/MAO	30	505,800	119	83.43	11.05	5.52	73.91	9.22	0.31	9.22	1.22	0.61	0.31	0.61	4.61
iPP5	**5**/MAO/PE	60	210,900	116	82.25	11.83	5.92	72.17	9.73	0.35	9.73	1.40	0.70	0.35	0.70	4.87
iPP6	**2**/MAO	60	166,400	111	76.95	15.37	7.68	64.54	11.82	0.59	11.82	2.36	1.18	0.59	1.18	5.91
iPP7	**4**/MAO	70	123,400	84	66.97	22.02	11.01	51.00	14.75	1.21	14.75	4.85	2.43	1.21	2.43	7.37

No or negligible regioerrors (2,1 insertions) could be observed in the ^{13}C NMR spectra of the samples [32,33].
[a] PP = polypropylene, PE = polyethylene.
[b] From the intrinsic viscosities.
[c] The melting temperatures were obtained with a differential scanning calorimeter Perkin–Elmer DSC-7 performing scans in a flowing N_2 atmosphere and heating rate of 10 °C/min.

was measured after 10 min. The tension set was calculated by using the following formula: $t_s(\varepsilon) = [(L_r - L_0)/L_0] \times 100$, whereas the elastic recovery was calculated as $r(\varepsilon) = [(L_f - L_r)/L_r] \times 100$.

Mechanical cycles of stretching and relaxation have been performed at room temperature on the stress-relaxed fibers and the corresponding hysteresis have been recorded. In these cycles the stress-relaxed fibers of i-PP samples, having the new initial length L_r, have been stretched up to the final lengths $L_f = 6L_0$ or $11L_0$, i.e. up to the elongation $\varepsilon = [(L_f - L_r)/L_r] \times 100$, and then relaxed at controlled rate. After each cycle, the values of the tension set have been measured. The final length of the relaxed specimens L_r' has been measured 10 min after the end of the relaxation step and the tension set has been calculated as: $t_s(\varepsilon) = [(L_r' - L_r)/L_r] \times 100$.

Values of tension set and elastic recovery have also been measured on unoriented compression-molded films of elastomeric samples after breaking. Specimens of initial length L_0 have been stretched up to the break. Ten minutes after breaking the two pieces of the sample have been fit carefully together so that they are in contact over the full area of the break and the final total length L_r of the specimen has been obtained by measuring the distance between the two bench marks. The tension set after breaking has been calculated as $t_b = [(L_r - L_0)/L_0] \times 100$, whereas the elastic recovery has been calculated as: $r_b = [(L_f - L_r)/L_r] \times 100$.

In the mechanical tests the ratio between the drawing rate and the initial length was fixed equal to 0.1 mm/(mm × min) for the measurement of Young's modulus and 10 mm/(mm × min) for the measurement of stress–strain curves and the determination of the other mechanical properties (stress and strain at break and tension set). The reported values of the mechanical properties are averaged over at least five independent experiments.

The stress-relaxation tests were performed on unoriented compression-molded films following the procedure described in the standard test method ASTM D2991-84. Instantaneous strains of 500 and 1000% were applied and the values of the stress were recorded as a function of the time.

3. Results and discussion

The i-PP samples were prepared using the metallocene catalysts of Chart 1 and are listed in Table 1. All samples are highly regioregular and contain only mistakes in the stereoregularity consisting in isolated *rr* triad defects and no measurable regioerrors. The amount of *rr* defects depend on the structure of the catalyst, in particular the indenyl substituents, and the conditions of polymerization and can be varied in the range between 0.5 and 11%. Correspondingly, the samples show melting temperatures variable between 162 and 80 °C (Table 1).

3.1. Unoriented samples

Samples used for the study of the structural transformations occurring during stretching and for the mechanical tests have been prepared by compression molding. The X-ray powder diffraction profiles of compression-molded films of some samples of Table 1 are reported in Fig. 1. The samples crystallize from the melt in mixtures of α- and γ-forms, the fraction of γ-form being dependent on the concentration of *rr* defects. The diffraction profiles of Fig. 1 present, indeed, both $(130)_\alpha$ and $(117)_\gamma$ reflections at $2\theta = 18.6$ and 20.1° of α- and γ-forms, respectively, the relative intensity of the $(117)_\gamma$ reflection of the γ-form increases with increasing concentration of *rr* defects.

The relative amount of γ-form, with respect to the α-form, is reported in Fig. 2 as a function of the concentration of *rr* defects. The most isotactic sample crystallizes basically in the α-form (Fig. 1(a)), with a limit low concentration of γ-form of 15–20%. The amount of γ-form increases with increasing content of *rr* defect up to 100% for *rr* contents higher than 6–7%. The more stereoirregular samples iPP5, iPP6 and iPP7, indeed, crystallize from the melt totally in the γ-form, as indicated by the high intensity of the $(117)_\gamma$ reflection of the γ-form at $2\theta = 20.1°$ and the absence of the $(130)_\alpha$ reflection of the α-form at $2\theta = 18.6°$ in the diffraction profiles d–f of Fig. 1.

Examples of stress–strain curves of compression-molded films of i-PP samples of Fig. 1, having different concentrations of *rr* defects and showing the mechanical behavior of stiff-plastic, highly flexible and elastomeric materials, are reported in Fig. 3 [13]. The values of the mechanical parameters (elastic modulus, stress and deformation at yield point and at break) evaluated from the stress–strain tests of all samples of Table 1 are reported in Table 2 and in Fig. 4 as a function of the concentration of *rr* defects.

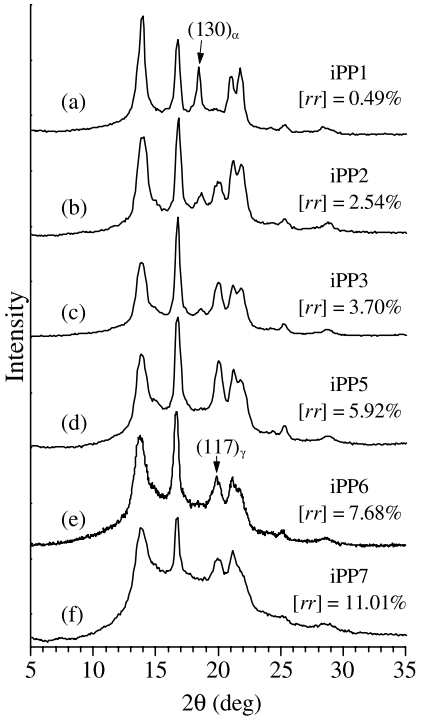

Fig. 1. X-ray powder diffraction profiles of i-PP samples of Table 1 crystallized from the melt by compression molding and cooling the melt to room temperature at 1 °C/min. The $(130)_\alpha$ reflection of the α-form at $2\theta = 18.6°$ and the $(117)_\gamma$ reflections of the γ-form at $2\theta = 20.1°$ are indicated.

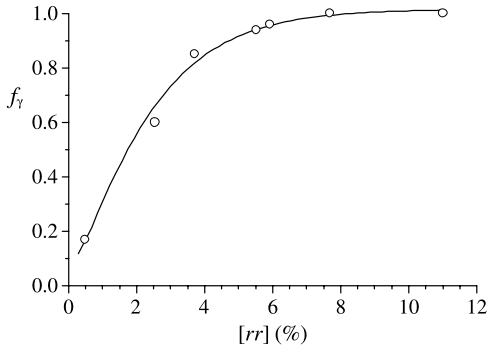

Fig. 2. Relative amount of γ-form, f_γ, in the i-PP samples of Table 1 crystallized from the melt by compression molding and cooling the melt to room temperature at cooling rate of 1 °C/min, as a function the concentration of *rr* defects.

The values of Young modulus (Fig. 4(A)) and stress at yielding (Fig. 4(B)) decrease, whereas the values of deformation at yield point and at break (Fig. 4(C)) increase with increasing concentration of *rr* defects and decreasing crystallinity (Table 2), indicating increase of ductility and toughness (Figs. 3 and 4(C)). Therefore, whereas samples with concentration of *rr* defects lower than 3–4% are stiff materials, samples with *rr* contents in the range 5–6% are highly flexible thermoplastic materials and, finally, elastomers can be obtained for concentrations of *rr* defects higher than 7% [13]. It is also apparent from Fig. 4(B) that the tensile strength strongly increases for very high concentrations of *rr* defects, due to the strong strain hardening at high deformation experienced by the lowest crystalline elastomeric sample containing the highest concentration of defects (sample iPP7 with [*rr*] = 11%, Figs. 3 and 4(B)).

The values of the tension set after breaking or after the deformation ε, reported in Table 2, clearly indicate a quite

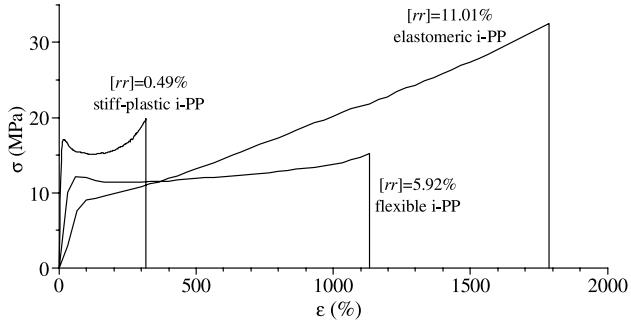

Fig. 3. Examples of stress–strain curves of unoriented compression molded films of three i-PP samples having different concentration of *rr* defects and showing mechanical properties of stiff-plastic, highly flexible and elastomeric materials.

Table 2
Elastic modulus (E), stress (σ_b) and strain (ε_b) at break, stress (σ_y) and strain (ε_y) at the yield point, tension set (t_b) and elastic recovery (r_b) after breaking, tension set after deformation of 500% ($t_s(500)$) and 1000% ($t_s(1000)$) and crystallinity (x_c) of unoriented compression molded films of i-PP samples prepared with catalysts of Chart 1

Samples	Catalyst	*rr* (%)	M_v	E (MPa)	σ_y (MPa)	ε_y (%)	σ_b (MPa)	ε_b (%)	t_b (%)	r_b (%)	$t_s(500)$ (%)	$t_s(1000)$ (%)	x_c (%)
iPP1	**1**/MAO	0.49	195,700	198±32	17±2	16±2	22±3	310±50	–	–			70
iPP2	**9**/MAO/PE	2.54	106,000	125±24	20±4	32±8	23±2	250±24	–	–			66
iPP3	**7**/MAO/PP	3.70	202,400	80±6	17±3	40±7	20±8	356±56	–	–			64
iPP4	**4**/MAO	5.52	505,800	70±9	12±3	45±5	15±2	454±50	–	–			60
iPP5	**6**/MAO/PE	5.92	210,900	64±6	12±1	50±1	16±2	1248±96	–	–			55
iPP6	**3**/MAO	7.68	166,400	27±6	10±2	60±6	22±4	850±140	580±92	40±5	337±25	–	45
iPP7	**5**/MAO	11.01	123,400	19±4	9±1	109±46	32±4	1787±214	381±3	292±10	184±39	494±15	42

The contents of *rr* defects and the molecular weights (M_v) of the samples are also indicated.

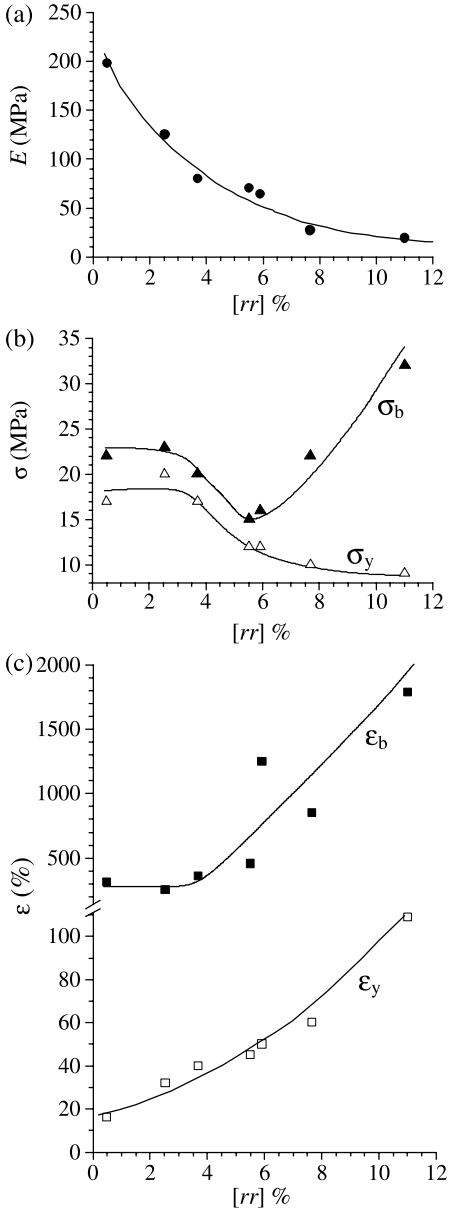

Fig. 4. Values of elastic modulus (A), stress (B) and deformation (C) at break (full symbols) and at yield point (open symbols) as a function of concentration of *rr* defects of i-PP samples of Table 1.

good elastic behavior of the two more steroirregular samples iPP6 and iPP7. In these materials the elastic properties are associated with remarkable values of the modulus of nearly 20–30 MPa (Table 2 and Fig. 4(A)), and, as discussed before, very high values of tensile strength, even higher than those of the more crystalline and isotactic samples (Figs. 3 and 4(B)).

This outstanding behavior is due to the fact that these samples are crystalline notwithstanding the low stereoregularity (Fig. 1). The presence of small crystalline domains induces elastomeric properties since crystals act as physical cross-links in the amorphous matrix. Moreover, a possible further crystallization and/or polymorphic

transformations that may occur during stretching play a fundamental role. In the next section this issue is analyzed showing a structural analysis of samples stretched at different deformations as in the stress–strain tests of Fig. 3. The presence of crystallinity gives high values of the strength (Table 2) and the possible further crystallization during stretching may explain the strong increase of the stress at high deformation observed for the more irregular sample iPP7 ([*rr*] = 11%).

3.2. Oriented fibers

Oriented fibers of the i-PP samples of Table 1 have been obtained by stretching at room temperature compression molded samples. As shown by the stress–strain curves of Fig. 3 even the most isotactic sample of Table 1 can be drawn at room temperature up to remarkable values of the strain (300–400%). This behavior is different from that of highly stereoregular commercial i-PP, prepared with Ziegler–Natta catalysts, which generally does not experience cold-drawing.

The X-ray fiber diffraction patterns, and the corresponding intensity profiles read along the equatorial line, of fibers of the most irregular sample iPP7, with content of *rr* defects of 11%, stretched at different values of deformation are reported in Fig. 5. As shown in Fig. 1, the initial unstretched compression-molded film of the sample iPP7 is in the γ-form (X-ray diffraction profile f of Fig. 1). The X-ray fiber diffraction patterns of fibers obtained at low deformations ($\varepsilon < 100\%$) present reflections at $2\theta = 14$ and 17° slightly polarized on the equator with a low degree of orientation of crystals (Fig. 5(A) and (B)). The absence or the very low intensity of the $(117)_\gamma$ reflection of the γ-form at $2\theta = 20°$, and of the $(130)_\alpha$ reflection of the α-form at $2\theta = 18.6°$, in the patterns of Fig. 5(A) and (B) indicate that the crystalline phase of fibers stretched at low deformations is characterized by disordered modifications intermediate between α- and γ-forms [8,10,12]. These disordered modifications of γ-form are characterized by defects in the regular packing of bilayers of chains with axes oriented alternatively along two nearly perpendicular directions, typical of the γ-form. Bilayers of chains succeed along a crystallographic direction with chain axes either parallel, as in the α-form, or perpendicular to each other, as in the γ-form [8]. This disorder produces a local situation of packing typical of the α-form, with some adjacent bilayers having parallel chains (α/γ disorder).

The patterns of Fig. 5(A) and (B) indicate that for the sample iPP7 the disordered modifications produced by stretching at low deformations present a prevalence of γ-like arrangement of chains with perpendicular axes. Therefore, only orientation of crystals of γ-form, or of α/γ disordered modifications, present in the unstretched film (Fig. 1(f)), is produced by stretching at low deformation.

The degree of orientation of crystals increases with increasing deformation ($\varepsilon \geq 100\%$), as indicated by the increase of the polarization of the reflections on the equator in the diffraction patterns of Fig. 5(C)–(E). Moreover the $(130)_\alpha$ reflection of the α-form at $2\theta = 18.6°$ appears starting from 100% deformation (Fig. 5(C)), and its intensity increases with further increasing deformation (Fig. 5(D) and (E)). This indicates that crystals of γ-form, or of α/γ disordered modifications, present in fibers stretched at low deformations (Fig. 5(A) and (B)), transform into α-form by stretching at higher deformations ($\varepsilon = 200$–600%). The diffraction patterns of Fig. 5(D) and (E) present, indeed, the three strong equatorial $(110)_\alpha$, $(040)_\alpha$ and $(130)_\alpha$ reflections at $2\theta = 14$, 16.8 and 18.6°, typical of the α-form. This structural transition involves transformation of modifications characterized by packing of perpendicular chains (γ-form) into crystals characterized by a prevalence of local packing with parallel chains, typical of the α-form.

The three equatorial 110, 040 and 130 reflections at $2\theta = 14$, 16.8 and 18.6° of the α-form transform into a broad halo in the range $2\theta = 14$–18° with further increasing deformation ($\varepsilon > 500$–600%), as shown in the X-ray diffraction patters of fibers stretched at $\varepsilon = 900$ and 1000% of Fig. 5(F) and (G). Moreover, reflections on the first layer line also transform into a broad halo centered at $2\theta = 21°$ (Fig. 5(G)). This indicates that crystals of α-form transforms into the mesomorphic form of i-PP [36]. At 1000% deformation fibers in the pure mesomorphic form of i-PP are obtained (Fig. 5(G)).

We recall that the mesomorphic form of i-PP is generally obtained by rapid quenching the melt to very low temperatures and is characterized by chains in the ordered three-fold helical conformation but high degree of disorder in the lateral packing of chains [36].

These data indicate that for the elastic sample iPP7, the easy deformation at high values of the draw ratio produces transformation of crystals of γ-form, present in the unstretched compression molded film (Fig. 1) and in fibers stretched at low deformations, into the α-form, which in turn transforms into the mesomorphic form at very high deformations.

This behavior provides an example of plastic deformation via necking (Fig. 3) of a semicrystalline bulk polymer accompanied by polymorphic transitions. Several molecular models of the plastic deformation have been discussed in the literature [37,38]. The occurrence of a polymorphic transition during deformation and the relationships between crystallographic features (for instance crystal symmetry and helical hands of the chain conformation) of the involved polymorphic forms, have been used to suggest an appropriate model. Peterlin has described the plastic deformation by a lamellae tilting and crystal shearing along the chain axes, followed by oriented rearrangement of these crystalline fragments [37]. A complete destruction of the crystalline lamellae followed by fibrillar recrystallization is suggested in other models [38]. Crystal–crystal transformations occurring during stretching in which helical conformations are involved are subjected to severe constraints. The major one is the need to preserve the initial

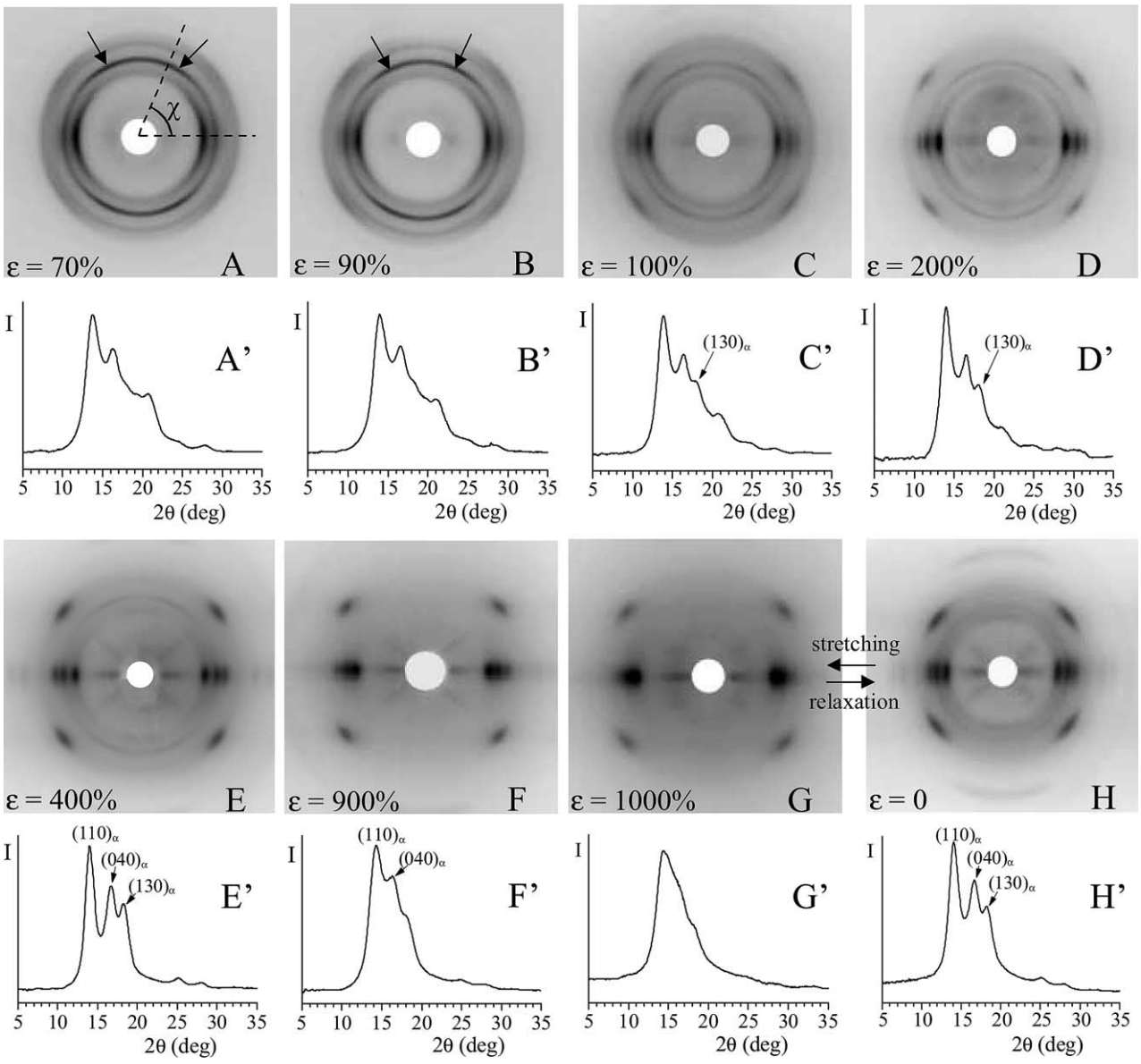

Fig. 5. X-ray fiber diffraction patterns (A)–(H), and corresponding profiles read along the equatorial lines (A′)–(H′), of fibers of the sample iPP7 with content of *rr* defects of 11.01%, obtained by stretching at room temperature compression molded films at values of the strain ε of 70% (A), 90% (B), 100% (C), 200% (D), 400% (E), 900% (F) and 1000% (G), and after releasing the tension from 1000% strain (*H*). The fiber in (G) is in the mesomorphic form, whereas the fiber in (H) is in the crystalline α-form. The $(110)_\alpha$, $(040)_\alpha$ and $(130)_\alpha$ reflections of the α-form at $2\theta = 14$, 17 and 18.6° are indicated. The azimuthal angle χ of the reflection at $2\theta = 17°$, indicated by arrows in (A) and (B), is defined in (A).

helical hand during the transformation process. Therefore, lamellae tilting and the shear mechanism cannot explain the change of handedness of a helical chain during the polymorphic transition. This is for instance the case of the observed transformation of the isochiral β-form of i-PP into the antichiral α-form by stretching [39]. Similar constraints are involved in the transformation of the γ-form into α-form [7,10,40]. In fact, even though both forms are characterized by a packing of right- and left-handed threefold helical chains with a similar stacking of ordered bilayers of enantiomorphic chains along the b_α and c_γ axes, in the α- and γ-forms, respectively [41], two consecutive bilayers are faced with chains of opposite chirality in the α-form and of the same chirality in the γ-form [41]. The transformation of γ- form into α-form occurring during stretching (Fig. 5) necessarily involves change of the chirality of helical chains and, therefore, cannot be explained by a simple lamellae tilting and crystal shearing along the chain axes. The γ-form transforms into the α-form through breaking of the lamellae and successive re-organization of the chains and fibrillar recrystallization with parallel chain axes oriented along the stretching direction. The fibrillar recrystallization may also produce increase of the total crystallinity by further crystallization of chains initially in the amorphous phase. This explains the strong strain-hardening observed in the stress–strain curve of the sample iPP7 (Figs. 3 and 4(B)).

At higher deformations the α-form transforms into the mesomorphic form (Fig. 5). This transformation has already been observed in the case of stretching at room temperature of i-PP samples prepared with Ziegler–Natta catalysts [42]. These studies by small angle and wide angle X-ray diffraction have indicated that there was no lamellar structure in the mesomorphic form of the i-PP fibers. It has been suggested that the formation of the mesophase is through the destruction of the lamellar crystalline phase, probably by pulling chains out from crystals, and the dominant constituent of the mesomorphic form may be oriented bundles of helical chains [42]. Also in the case of the elastomeric sample iPP7 of Fig. 5, we can assume that, after formation of fibers in the α-form at 400–500% deformation, the chains are pulled out from the lamellae of α-form by further stretching at higher deformation and re-organize forming crystalline mesomorphic aggregates characterized by chains in 3/1 helical conformation, where the parallelism of the chain axes is maintained and only a poor correlation in the lateral positioning of the chain axes is present.

It is worth noting that in the X-ray fiber diffraction patterns of fibers of the sample iPP7 stretched at low deformations ($\varepsilon \leq 100\%$, Fig. 5(A)–(C)) the second equatorial reflection at $2\theta = 17°$, corresponding to the $(040)_\alpha$ reflection for the α-form and the $(008)_\gamma$ reflection for the γ-form, appears polarized either on the equator, or on off-equatorial layer lines on the region close to the meridian (reflections indicates by arrows in Fig. 5(A) and (B)). The position of this reflection may be indicated by the azimuthal coordinate χ defined in Fig. 5(A) ($\chi = 0$ and 90° for equatorial and meridional reflections, respectively). The distribution of the intensity of the reflection at $2\theta = 17°$ along the azimuthal arc in the X-ray fiber diffraction patterns of Fig. 5 is reported in Fig. 6 for fibers stretched at different values of deformation. It is apparent that for low deformations the azimuthal profiles of Fig. 6(b)–(d) present diffraction maxima at $\chi \approx 60$ and 120°, symmetric with respect to the meridional position at $\chi = 90°$, besides to the equatorial maxima at $\chi = 0$ and 180°. The intensity of the maxima at $\chi \approx 60$ and 120° on off-equatorial layer lines decreases, whereas that on the equator at $\chi = 0$ and 180° increases with increasing deformation (Fig. 6(e)–(i)). At very high deformation ($\varepsilon > 700\%$) the reflection at $2\theta = 17°$ is polarized only on the equator and only the corresponding diffraction maxima at $\chi = 0$ and 180° are observed in the azimuthal profiles of Fig. 6(h) and (i).

The $(040)_\alpha$ or $(008)_\gamma$ reflection at $2\theta = 17°$ corresponds to crystallographic planes perpendicular to the direction of stacking of bilayers, that is perpendicular to the b_α axis in the α-form, or to the c_γ axis in the γ-form. The polarization of this reflection on off-equatorial layer lines at $\chi = 60$ and 120° (Figs. 5(A), (B) and 6(b)–(d)) indicates that crystals are oriented with the axes of stacking of bilayers of chains (c_γ axis of the γ-form) aligned preferably along the stretching direction (as shown in Fig. 7 for the γ-form), precisely at nearly 30° to the stretching direction [12]. In this orientation the polymeric chains are oriented in directions nearly perpendicular to the stretching direction. The presence of diffraction maxima also on the equator at $\chi = 0$ and 180° (Figs. 5(A), (B) and 6(b)–(d)) indicates that a fraction of crystals with chain axes oriented along the stretching direction are also present. These crystals are probably in α/γ disordered modifications closer to the α-form with high fraction of consecutive bilayers having parallel chains, as in the α-form.

This non-standard fiber orientation is achieved before necking ($\varepsilon < 100\%$, Fig. 3) and, therefore, can be obtained through lamellar tilting and crystal shearing. At higher deformations the amount of crystals oriented with chains axes nearly perpendicular to the stretching direction decreases with increasing deformation, as indicated by the decrease of the intensity of the $(040)_\alpha$ or $(008)_\gamma$ reflection at

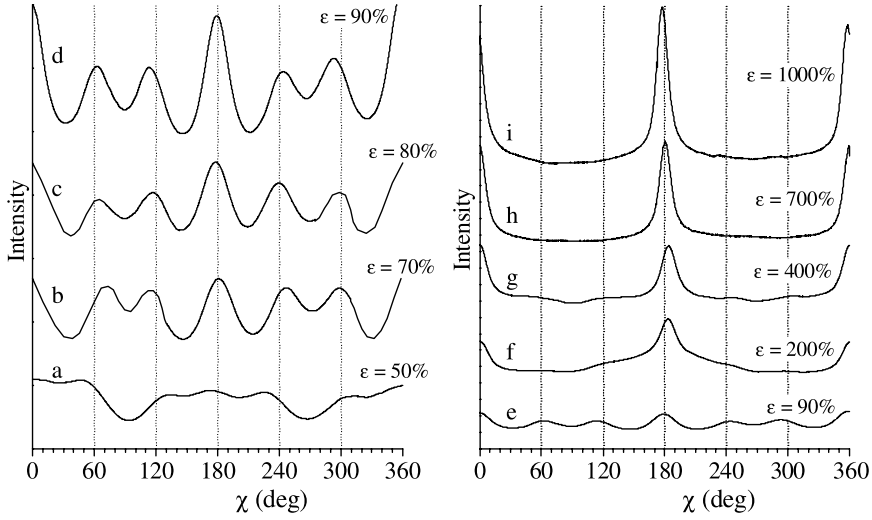

Fig. 6. X-ray diffraction azimuthal profiles of the reflection at $2\theta = 17°$ in the fiber diffraction patterns of Fig. 5 of fibers of the sample iPP7 with $[rr] = 11.01\%$ stretched at the indicated values of the deformation ε. The azimuthal scan at deformation $\varepsilon = 90\%$ is reported in two different intensity scales (profiles d,e).

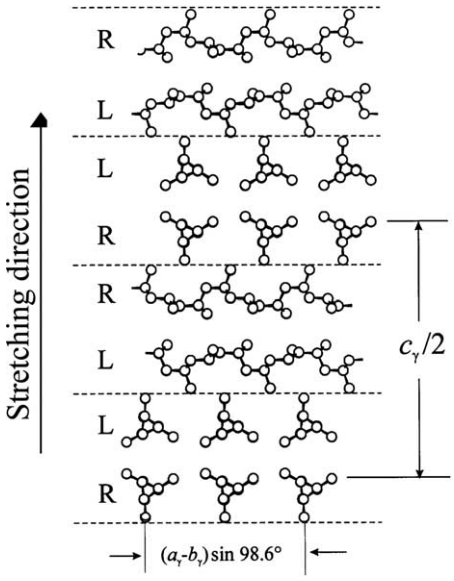

Fig. 7. Model of packing of i-PP chains in the γ-form. The dashed horizontal lines delimit bilayers of chains and are parallel to the $(008)_\gamma$ crystallographic planes. a_γ, b_γ and c_γ are the unit cell parameters of the orthorhombic unit cell of γ-form [41]. R and L identify rows of all right- and all left-handed 3/1 helical chains, respectively. In fibers of Fig. 5(A) and (B) the c_γ axis is oriented along the stretching direction, hence the chain axes are nearly perpendicular to the stretching direction.

$\chi \approx 60$ and 120°, on off-equatorial layer lines, and the increase of the intensity on the equator at $\chi = 0$, with increasing deformation ($\varepsilon > 100\%$, Figs. 5(B)–(H) and 6(e)–(i)). In the necking zone the breaking of the lamellae and successive fibrillar recrystallization produce standard fiber orientation with parallel chain axes oriented along the stretching direction and, contemporarily, the transformation of γ-form crystals into α-form.

The X-ray diffraction pattern, and the corresponding equatorial profile, of fibers of the sample iPP7 stretched at 1000% elongation (Fig. 5(G)), after releasing the tension, are reported in Fig. 5(H) and (H′), respectively. It is apparent that the mesomorphic form (Fig. 5(G)) transforms into the α-form of i-PP upon releasing the tension, as indicated by the presence of the $(110)_\alpha$, $(040)_\alpha$ and $(130)_\alpha$ reflections at $2\theta = 14$, 17 and 18.6°, typical of the crystalline α-form, in the diffraction pattern of Fig. 5(H) and (H′). This transformation is reversible upon successive stretching and relaxing cycles. The crystalline α-form transforms by stretching into the disordered mesomorphic form, which, in turn, transforms back into the α-form by releasing the tension (Fig. 5(G) and (H)).

As shown in the previous section the sample iPP7 show elastic behavior, hence, after removing the tension in fibers stretched up to 1000% deformation a recovery of the initial dimension is observed. The data of Fig. 5 indicate that in correspondence to this elastic recovery a reversible polymorphic transition of the mesomorphic form into the crystalline α-form occurs. It is worth noting that the transformation of the mesomorphic disordered form into the α-form corresponds to an increase of crystalline order. The crystallization upon removing the tension in stretched fibers is not common in polymers and is opposite to what is generally observed in a common elastomer as the natural rubber, for which crystallization occurs during stretching, whereas melting occurs upon releasing the tension [43,44].

Similar behavior has been observed for the other elastomeric sample iPP6 having content of *rr* defect of 7.68%. The X-ray diffraction patterns, and the corresponding equatorial profiles, of fibers of the sample iPP6 stretched at different values of deformation are reported in Fig. 8. Also for this samples the initial unstretched compression-molding film is in the γ-form (Fig. 1(e)). The diffraction patterns of fibers stretched at low deformations, up to $\varepsilon = 300\%$ (Fig. 8(A)), present reflections of the γ-form with the $(008)_\gamma$ reflection at $2\theta = 17°$ polarized on the equator at $\chi = 0$ and on off-equatorial layer lines at $\chi = 60$ and 120°, indicating, also in this case, orientation of crystals of γ-form with the c_γ axis aligned nearly along the stretching direction, as in Fig. 7.

Crystals of γ-form partially transform into α-form with increasing deformation ($\varepsilon = 400\%$), as indicated by the presence of $(110)_\alpha$, $(040)_\alpha$ and $(130)_\alpha$ reflections of the α-form at $2\theta = 14$, 17 and 18.6° in the diffraction pattern of Fig. 8(B), or in α/γ disordered modifications closer to the α-form. A fraction of crystals of γ-from or of α/γ disordered modifications with crystals oriented with the c_γ axis aligned along the stretching direction, is still present, as indicated by the non-negligible intensity of the reflection at $2\theta = 17°$ on off-equatorial layers at $\chi = 60$ and 120° (Fig. 8(B)). At very high deformation, $\varepsilon > 500$–600%, the α-form transforms into the mesomorphic form and the $(110)_\alpha$, $(040)_\alpha$ and $(130)_\alpha$ reflections transform into a broad halo in the range of $2\theta = 14$–18°. This transformation is complete at the limit of deformation of the sample at $\varepsilon = 600$–800% (Fig. 8(C)).

Also for the sample iPP6 the mesomorphic form partially crystallize in the α-form upon releasing the tension, as indicated by the better resolution of the $(110)_\alpha$, $(040)_\alpha$ and $(130)_\alpha$ reflections in the X-ray diffraction pattern of Fig. 8(D), and, correspondingly, the fiber experiences elastic recovery.

It is worth noting that a similar elastomeric behavior has been observed for much more stereoirregular i-PP samples prepared with a C_2-symmetric metallocene catalyst [12,13]. For instance a poorly isotactic polypropylene having concentration of the isotactic *mmmm* pentad of 35%, much lower than that of the sample iPP7 ([*mmmm*] = 51%, Table 1), and a total content of *rr* triad defects of 16%, higher than that of the sample iPP7 ([*rr*] = 11%), shows outstanding elastic properties [12]. However, in this case a completely different polymorphic behavior during tensile deformation has been observed [12]. Due to the high concentration of defects this sample is essentially amorphous and does not crystallize from the melt. It slowly crystallizes upon aging at room temperature or by stretching

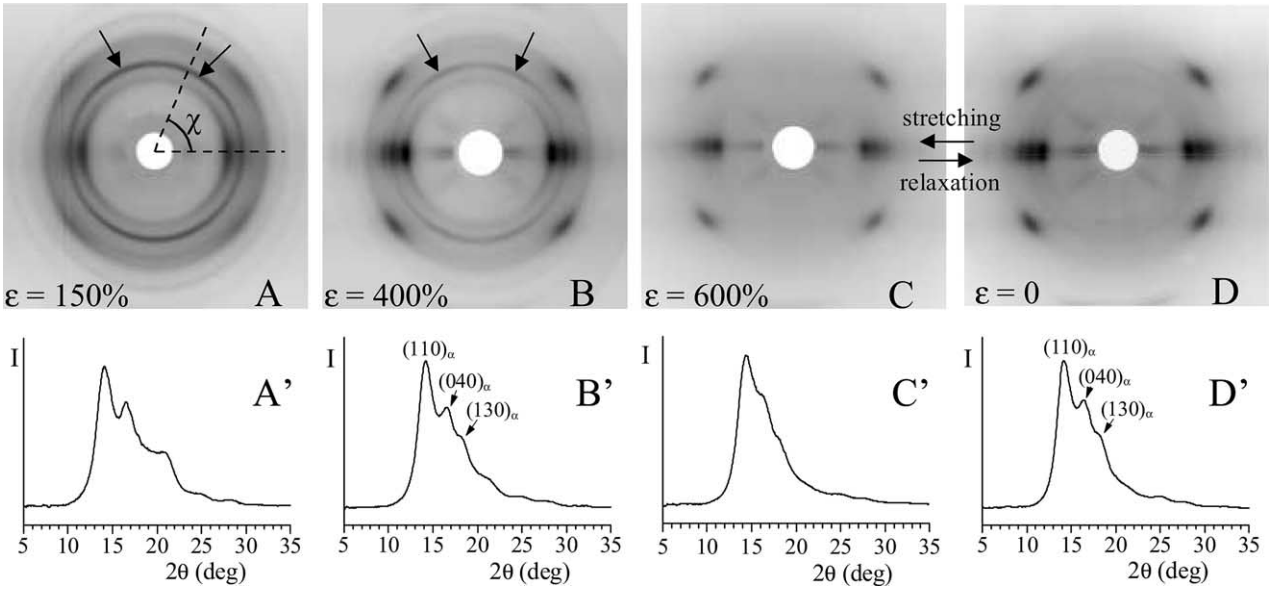

Fig. 8. X-ray fiber diffraction patterns (A)–(D), and corresponding profiles read along the equatorial lines (A′)–(D′), of fibers of the sample iPP6 with content of *rr* defects of 7.68%, obtained by stretching at room temperature compression molded films at values of the strain ε of 150% (A), 400% (B) and 600% (C), and after releasing the tension (D). The $(110)_\alpha$, $(040)_\alpha$ and $(130)_\alpha$ reflections of the α-form at $2\theta = 14$, 17 and 18.6° are indicated. The azimuthal angle χ of the reflection at $2\theta = 17°$, indicated by arrows in (A) and (B), is defined in (A).

in disordered modifications intermediate between the α- and γ-forms, with a maximum degree of crystallinity of only 16% and a melting temperature of 45 °C [12]. The stretching of this sample even at high deformation does not produce formation of the α-form or the mesomorphic form, as instead occurs for the samples iPP7 and iPP6, but only α/γ disordered modifications, more similar to the α-form, are obtained [12]. This different behavior is due to the very short length of the regular isotactic sequences, the average value being only five monomeric units [23]. For this reason the pure α-form is never obtained and, even at high deformation, a not negligible fraction of bilayers of chains arranged with non parallel chain axes as in the γ-form is always present [8,12]. In this sample the elastic properties are associated to the reversible transformation between α/γ disordered modifications having high fraction of α-like arrangements with parallel chains (obtained by stretching) and modifications having high fraction of γ-like arrangements with perpendicular chains (obtained after relaxation) [12]. This confirms that polypropylenes of different stereoregularity, containing different concentrations of stereodefects, may exhibit completely different crystallization properties and deformation behavior, so that they should be considered as different materials showing different mechanical properties.

The stress–strain tests of Fig. 3 have shown that the slightly more stereoregular sample iPP5, with *rr* content of 5.92%, behaves as a highly flexible materials, since it can be stretched up to very high deformations (higher than 1000%), but does not show elastic properties. The structural evolution of the sample iPP5 during stretching is reported in Fig. 9. Crystals of the γ-form present in the unstretched film (profile d in Fig. 1) are oriented at low deformations as in Fig. 7, with the c_γ axes oriented at nearly 30° to the stretching direction, as indicated by the polarization of the $(008)_\gamma$ reflection at $2\theta = 17°$ on off-equatorial layer lines at $\chi = 60$ and 120° in the diffraction pattern of Fig. 9(A). At higher values of deformation, instead of formation of the α-form, as occurs for the samples iPP7 and iPP6 (Figs. 5 and 8), a transformation of the γ-form into the mesomorphic form is observed. It is apparent from Fig. 9(B), indeed, that the formation of the broad halo on the equator in the range of $2\theta = 14$–18°, typical of the mesomorphic form, is observed already at 300% deformation. Crystals of γ-form oriented as in Fig. 7 are, however, still present, along with the mesomorphic form, up to 500% deformation, as indicated by the presence of the reflection at $2\theta = 17°$ polarized on off-equatorial layer lines at $\chi \approx 60$ and 120° in the diffraction patterns of Fig. 9(B) and (C). At the highest deformation ($\varepsilon > 500\%$) a pure mesomorphic form is obtained (Fig. 9(D)). At variance with the elastic samples iPP6 and iPP7, no polymorphic transition is observed for the sample iPP5 upon releasing the tension from fibers stretched at the highest deformation. The mesomorphic form obtained by stretching at high deformation (Fig. 9(D)) does not transform into the α-form by removing the tension, as instead occurs for samples iPP6 and iPP7, and the relaxed fiber remains in the mesomorphic form. Correspondingly no elastic recovery of the fibers is observed.

These data indicate that when the sample experiences elastic recovery after releasing the tension in stretched fibers, a polymorphic transition between the mesomorphic form and the α-form is also observed. When the sample does not show elastic recovery, no polymorphic transition occurs.

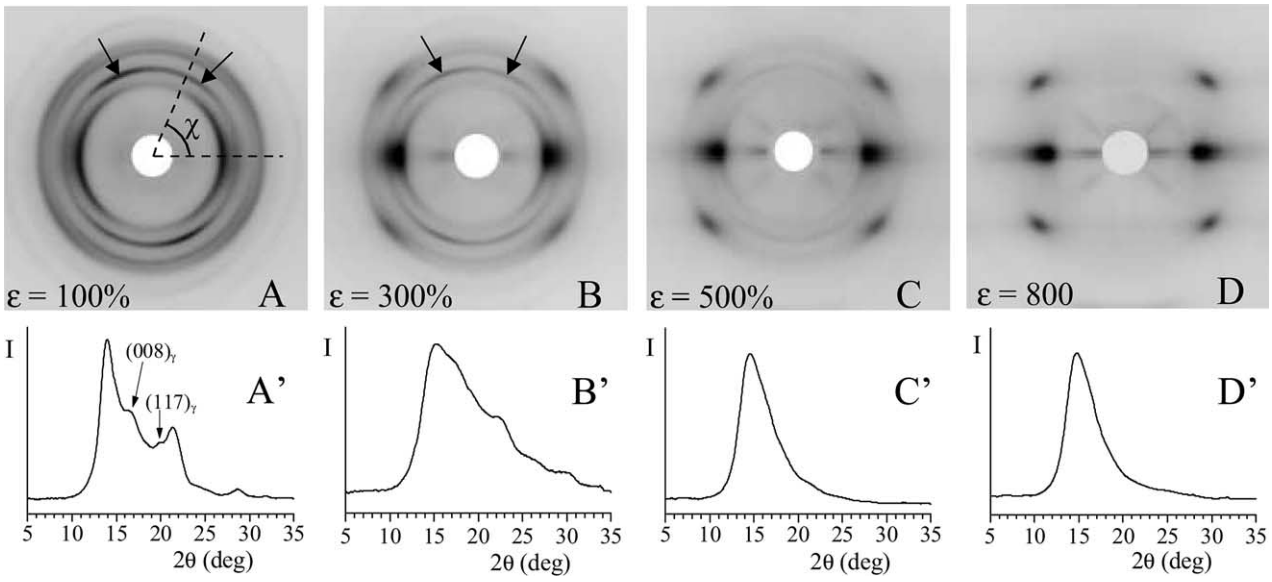

Fig. 9. X-ray fiber diffraction patterns (A)–(D), and corresponding profiles read along the equatorial lines (A′)–(D′), of fibers of the sample iPP5 with content of *rr* defects of 5.92%, obtained by stretching at room temperature compression molded films at values of the strain ε of 100% (A), 300% (B), 500% (C) and 800% (D). The $(110)_\alpha$, $(040)_\alpha$ and $(130)_\alpha$ reflections of the α-form at $2\theta = 14$, 17 and 18.6° are indicated. The azimuthal angle χ of the reflection at $2\theta = 17°$, indicated by arrows in (A) and (B), is defined in (A).

Therefore, the elasticity in metallocene-made isotactic polypropylene, at least in these samples, is always associated with a reversible polymorphic transition.

For all the other more stereoregular i-PP samples of Table 1, with contents of *rr* defects lower than 5%, compression-molded unstretched films are generally in mixtures of α- and γ-forms (Fig. 1(b) and (c)), whereas the most isotactic sample iPP1 is basically in the α-form (Fig. 1(a)). These samples can be easily stretched up to 200–300% deformation (Fig. 3). At the maximum possible value of deformation crystals of α- or γ-forms transform into the mesomorphic form of i-PP. The X-ray diffraction patterns of fibers of the samples iPP1, iPP2 and iPP3 with *rr* contents of 0.49, 2.54 and 3.70%, respectively, stretched at the maximum deformation are reported in Fig. 10. It is apparent that in the diffraction patterns of fibers of the most stereoregular samples iPP1 and iPP2 (Fig. 10(A) and (B), respectively), even at the maximum deformation, along with the broad halo in the range of $2\theta = 14$–18° of the mesomorphic form, non-oriented reflections of the α-form (for the sample iPP1, Fig. 10(A)) and of both α- and γ-forms (for the sample iPP2, Fig. 10(B)) are present.

This indicates that along with oriented crystals of the mesomorphic form, a fraction of non-oriented crystals of α- or γ-forms are still present. In the case of the most isotactic sample iPP1 these crystals are basically in the α-form, whereas for the more irregular sample iPP3 they are mainly in the γ-form or in disordered α/γ modifications. The stretching at room temperature of these samples, therefore, does not produce a high orientation of crystals, probably because of the limited possible deformation. Crystals that undergo plastic deformation and achieve orientation, rapidly transform into the mesomorphic form, whereas non-deformed crystals remain in the crystalline forms (α- or γ-forms) of the initial unoriented film. Also in these samples that behave as stiff-plastic materials with no elastic properties, the mesomorphic form does not transform into the α-form upon removing the tension.

The analysis of the mechanical properties (Fig. 3 and Table 2) and the structural characterization of the most irregular elastomeric samples iPP6 and iPP7 (Figs. 5 and 8) has shown that, because of the presence significant level of crystallinity, unoriented films undergo irreversible plastic deformation, involving structural and morphological transformations. This explains the relatively high values of tension set measured after breaking or after a given deformation (Table 2), which indicate a non-complete elastic recovery after the first stretching. In particular the more crystalline sample iPP6 presents an elastic recovery lower than that of the sample iPP7 (Table 2).

Strained and stress-relaxed fibers of the samples iPP6 and iPP7, that have already undergone plastic deformation, present instead complete elastic recovery. To quantify the elastic behavior mechanical cycles of stretching and relaxation have been performed at room temperature on oriented stress-relaxed fibers of the samples iPP6 and iPP7, and the corresponding hysteresis and values of tension set have been measured. These fibers have been obtained by stretching compression-molded films at 500 and 1000% deformations, up to final lengths of $L_f = 6L_0$ and $11L_0$ with L_0 the initial length of the unoriented film, and then removing the tension, allowing the fibers to relax. The values of tension set $t_s(\varepsilon)$ observed after this first stretching up to $\varepsilon = 500$ and 1000% are similar to those observed after

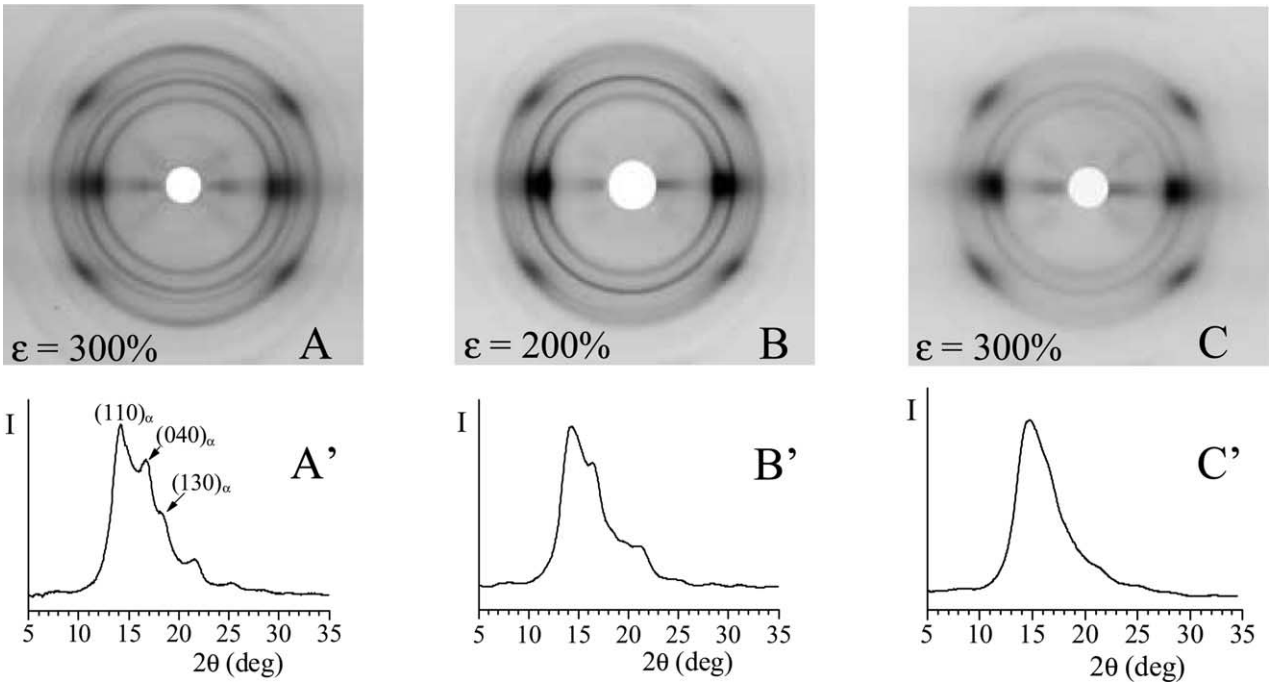

Fig. 10. X-ray fiber diffraction patterns (A)–(C), and corresponding profiles read along the equatorial lines (A′)–(C′), of fibers of the sample iPP1 with [*rr*] = 0.49% (A), iPP2 with [*rr*] = 2.54% (B) and iPP3 with [*rr*] = 3.70% (C) obtained by stretching at room temperature compression molded films at the indicated values of the strain ε. The $(110)_\alpha$, $(040)_\alpha$ and $(130)_\alpha$ reflections of the α-form at $2\theta = 14$, 17 and 18.6° are indicated.

breaking and are also reported in Table 2 ($t_s(500) = 337$ and 184% for the samples iPP6 and iPP7, respectively, and $t_s(1000) = 494\%$ for the sample iPP7). These fibers have been identified as iPP6-500 for the sample iPP6, and iPP7-500 and iPP7-1000 for the sample iPP7. As shown in Figs. 5 and 8 these stress-relaxed fibers are in the α-form.

The hysteresis cycles, composed of the stress–strain curves measured during the stretching of the fiber iPP7-1000, immediately followed by the curves measured during the relaxation at controlled rate, are reported in Fig. 11 as an example.

The values of tension set and dissipated energy measured after each cycle are reported in Table 3. It is apparent that for both samples iPP6 and iPP7, either the tension set or the dissipated energy decreases in successive cycles. The tension set measured after the third cycle is zero, successive hysteresis cycles, measured after the third one, being all nearly coincident, indicating a perfect elastic recovery.

Both fibers of samples iPP6 and iPP7 present, therefore, good elastic properties; since the unstretched compression molded film of the sample iPP6 presents elastic recovery after the first stretching better than that of the sample iPP6 (the tension set after stretching unoriented films of the samples iPP7 and iPP6, up to 500% deformation, being 184 and 337%, respectively), fibers of the more irregular sample iPP7 show elastic behavior in a deformation range larger than that of fibers of the sample iPP6.

The remarkable values of the strength of the elastomeric samples iPP6 and iPP7 are probably related to the increase of crystallinity and the structural transitions occurring during stretching. Moreover the formation of the metastable mesomorphic form at high deformation and the successive crystallization upon relaxation may play an important role. As shown by the structural analysis of Figs. 5 and 8 the elastic behavior of these poorly isotactic polypropylene samples is associated with a reversible polymorphic transition between the α-form and the mesomorphic form of i-PP, which occurs during successive stretching and relaxation cycles of Fig. 11. When the sample does not experiences elastic recovery, as in the case of the slightly

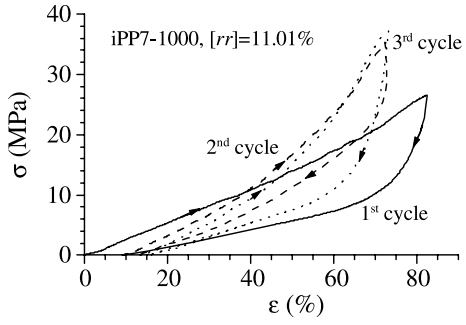

Fig. 11. Stress–strain hysteresis cycles recorded at room temperature, composed of stretching and relaxation (at controlled rate) steps according to the direction of the arrows, for the stress-relaxed fiber iPP7-1000 of the sample iPP7 with content of *rr* defects of 11.01%. The stress-relaxed fiber has been prepared by stretching compression-molded films, of initial length L_0, up to 1000% elongation (final length $L_f = 11L_0$), and, then, removing the tension. In the hysteresis cycles the stretching steps are performed stretching the fibers up to final length $L_f = 11L_0$. Continuous lines: first cycle; dashed lines: second cycle; dotted lines: third cycle and successive cycles.

Table 3
Values of the tension set (t_s) and the dissipated energy (E_{diss}) measured in the hysteresis cycles for stress-relaxed fibers of the samples iPP6 and iPP7

Sample	t_s (%) I cycle	t_s (%) II cycle	t_s (%) III cycles	t_s (%) IV cycle	$\langle E_{diss}\rangle$ (%) I cycle	$\langle E_{diss}\rangle$ (%) II cycle	$\langle E_{diss}\rangle$ (%) III cycle	$\langle E_{diss}\rangle$ (%) IV cycle
iPP6-500	6.5	2.5	0	0	66	62	60	60
iPP7-500	8.4	2.3	0	0	54	49	44	44
iPP7-1000	7.8	3.6	1.7	0	52	50	43	21

more isotactic sample iPP5, which behaves as a highly flexible thermoplastic material, the crystallization of the mesomorphic form into α-form is no longer observed.

3.3. Stress-relaxation tests for unoriented films

Stress-relaxation experiments have been performed at room temperature on the compression molded films of the elastomeric sample iPP7 with [*rr*] = 11.01% to test the strength of these materials in conditions of deformations for long time. In the stress-relaxation curves of the sample iPP7, reported in Fig. 12, the values of the stress are recorded as a function of time after application on compression molded films of instantaneous strains of 500 and 1000%.

The samples show a typical behavior of viscoelastic materials. A loss of the stress of 50–60% after nearly 300 s, regardless of the values of the instantaneous deformation, is observed. Then the stress remains constant at values as high as 4–6 MPa for long time. These data confirm the previous observations that these poorly isotactic samples show at room temperature high toughness and ductility and remarkable strength even when stresses are applied for long time.

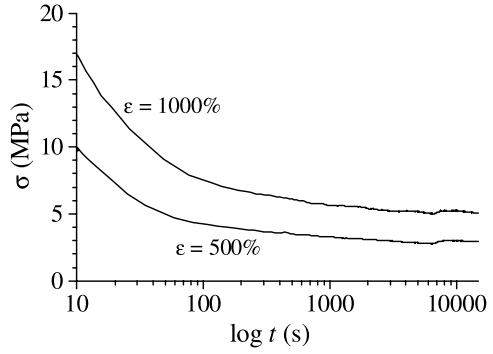

Fig. 12. Stress-relaxation curves of sample iPP7 with content of *rr* defect of 11.01%. The values of the stress are reported as a function of time for compression molded films after application of instantaneous strains of 500 and 1000%.

4. Conclusions

The plastic deformation of isotactic polypropylene prepared with metallocene catalysts and the polymorphic transformations occurring during deformation have been studied. The influence of the presence of defects of stereoregularity (isolated *rr* triad defects) on the deformation behavior has been analyzed through the study of the structure and the mechanical properties of highly regioregular isotactic polypropylene with variable stereoregularity, containing only *rr* stereo-defects in a wide range of concentration, with melting temperatures ranging between 162 and 80 °C, have been obtained.

Different concentrations of *rr* defects induce different crystallization behavior and different physical properties. Samples with low concentration of *rr* defects, up to 3–4%, present high melting temperatures, in the range 162–130 °C, and behave as stiff plastic materials. Sample with higher *rr* content, in the range 4–6% and melting temperatures around 115–120 °C are highly flexible thermoplastic materials, showing very high deformation at break. Samples with concentration of *rr* defects in the range 7–11% and melting temperature in the range 80–110 °C are thermoplastic elastomers with high strength.

The outstanding properties of the more stereoirregular and elastomeric samples are related to the further crystallization and structural transitions occurring during stretching. For the elastomeric samples the γ-form present in the unstretched compression-molded film transforms by stretching into the α-form, which in turn transforms into the mesomorphic form at very high deformation. The mesomorphic form transforms back into the crystalline α-form upon releasing the tension. Correspondingly elastic recovery of the initial dimension of the samples is observed. Due to the relatively low crystallinity and small crystal sizes, the molecules become suddenly free to reorganize and crystallize in the most stable α-form when the tension is removed.

The transformation of α- or γ-form into the mesomorphic form by stretching is also observed for the more crystalline and stereoregular samples. However, since the level of crystallinity is too high, and/or the size of crystals is too large, these samples do not show elastic behavior but behave as flexible or stiff-plastic materials and the crystallization of the mesomorphic form into the α-form upon releasing the tension is no longer observed. When the samples are rigid in their stretched state even after removing the tension, the mesomorphic form does not crystallize into the α-form.

These data indicates that the elastic behavior of less crystalline and stereoregular samples iPP6 and iPP7 is always associated to a reversible polymorphic transition between the mesomorphic form and the α-form of i-PP.

These samples show elastic behavior because the degree of crystallinity and the size of crystals are lower than in the case of more stereoregular samples. However, since elasticity is generally a property of the amorphous phase, and the degree of crystallinity of samples iPP6 and iPP7 is still relatively high (≈40%), probably elasticity in these samples is partially due to the enthalpic contribution associated with the crystallization of the mesomorphic form into the α-form occurring upon releasing the tension.

Acknowledgements

Financial supports from Basell Polyolefins (Ferrara, Italy) and from the 'Ministero dell'Istruzione, dell'Università e della Ricerca' of Italy (PRIN 2004 project) are gratefully acknowledged.

References

[1] Ewen JA, Elder MJ, Jones RL, Haspeslagh L, Atwood JL, Bott SJ, et al. Makromol Chem Macromol Symp 1991;48/49:253.
[2] Brintzinger HH, Fischer D, Mulhaupt R, Rieger B, Waymouth RM. Angew Chem Int Ed Engl 1995;34:1143.
[3] Kaminsky W. Macromol Chem Phys 1996;197:3907.
[4] Resconi L, Cavallo L, Fait A, Piemontesi F. Chem Rev 2000;100: 1253.
[5] Fischer D, Mülhaupt R. Macromol Chem Phys 1994;195:1433.
[6] Thomann R, Wang C, Kressler J, Mulhaupt R. Macromolecules 1996; 29:8425.
[7] Alamo RG, Kim MH, Galante MJ, Isasi JR, Mandelkern L. Macromolecules 1999;32:4050.
[8] Auriemma F, De Rosa C, Boscato T, Corradini P. Macromolecules 2001;34:4815.
[9] De Rosa C, Auriemma F, Circelli T, Waymouth RM. Macromolecules 2002;35:3622.
[10] Auriemma F, De Rosa C. Macromolecules 2002;35:9057.
[11] De Rosa C, Auriemma F, Circelli T, Longo P, Boccia AC. Macromolecules 2003;36:3465.
[12] De Rosa C, Auriemma F, Perretta C. Macromolecules 2004;37:6843.
[13] De Rosa C, Auriemma F, Di Capua A, Resconi L, Guidotti S, Camurati I, et al. J Am Chem Soc 2004;126:17040.
[14] Spaleck W, Küber F, Winter A, Rohrmann J, Bachmann B, Antberg M, et al. Organometallics 1994;13:954.
[15] Resconi L, Piemontesi F, Camurati I, Sudmeijer O, Nifant'ev IE, Ivchenko PV, et al. J Am Chem Soc 1998;120:2308.
[16] Resconi L, Balboni D, Baruzzi G, Fiori C, Guidotti S, Mercandelli P, et al. Organometallics 2000;19:420.
[17] (a) Mallin DT, Rausch MD, Lin Y-G, Dong S, Chien JCW. J Am Chem Soc 1990;112:2030.
(b) Chien JCW, Llinsas GH, Rausch MD, Lin G-Y, Winter HH. J Am Chem Soc 1991;113:8569.
(c) Chien JCW, Llinsas GH, Rausch MD, Lin G-Y, Winter HH, Atwood JL, et al. J Polym Sci Polym Chem 1992;30:2601.
(d) Llinas GH, Day RO, Rausch MD, Chien JCW. Organometallics 1993;12:1283.
[18] (a) Gauthier WJ, Collins S. Macromol Symp 1995;98:223.
(b) Gauthier WJ, Corrigan JF, Taylor NJ, Collins S. Macromolecules 1995;28:3771.
(c) Gauthier WJ, Collins S. Macromolecules 1995;28:3779.
(d) Bravakis AM, Bailey LE, Pigeon M, Collins S. Macromolecules 1998;31:1000.
[19] (a) Dietrich U, Hackmann M, Rieger B, Klinga M, Leskelä M. J Am Chem Soc 1999;121:4348.
(b) Müller G, Rieger B. Prog Polym Sci 2002;27:815.
(c) Rieger B, Troll C, Preuschen J. Macromolecules 2002;35: 5742.
[20] Resconi L, Jones RL, Rheingold A, Yap GPA. Organometallics 1996; 15:998.
[21] Resconi L. Synthesis of atactic polypropylene using metallocene catalysts. In: Kaminsky W, Scheirs J, editors. Metallocene-based polyolefins. Preparation, properties, technology. New York: Wiley; 1999. p. 467.
[22] Resconi L, Silvestri R. In: Salamone JC, editor. The polymeric materials encyclopedia. Boca Raton: CRC Press; 1996. p. 6609.
[23] Balboni D, Moscardi G, Baruzzi G, Braga V, Camurati I, Piemontesi F, et al. Macromol Chem Phys 2001;202:2010.
[24] Resconi L, Moscardi G, Silvestri R, Balboni D. PCT Int Appl WO 00/01738. Montell, Italy; 2000.
[25] (a) Coates GW, Waymouth RM. Science 1995;267:217.
(b) Hu Y, Krejchi MT, Shah CD, Myers CL, Waymouth RM. Macromolecules 1998;31:6908.
(c) Lin S, Waymouth RM. Acc Chem Res 2002;35:765.
[26] VanderHart DL, Alamo RG, Nyden MR, Kim MH, Mandelkern L. Macromolecules 2000;33:6078.
[27] Alamo RG, VanderHart DL, Nyden MR, Mandelkern L. Macromolecules 2000;33:6094.
[28] Thomann R, Semke H, Maier RD, Thomann Y, Scherble J, Mülhaupt R, et al. Polymer 2001;42:4597.
[29] Hosier IL, Alamo RG, Esteso P, Isasi GR, Mandelkern L. Macromolecules 2003;36:5623.
[30] Nifant'ev IE, Guidotti S, Resconi L, Laishevtsev I. PCT Int Appl WO 01/47939. Basell, Italy; 2001.
[31] Resconi L, Guidotti S, Camurati I, Nifant'ev IE, Laishevtsev I. Polym Mater Sci Eng 2002;87:76.
[32] Fritze C, Resconi L, Schulte J, Guidotti S. PCT Int Appl WO 03/00706. Basell, Italy; 2003.
[33] (a) Nifant'ev IE, Laishevtsev IP, Ivchenko PV, Kashulin IA, Guidotti S, Piemontesi F, et al. Macromol Chem Phys 2004;205: 2275.
(b) Resconi L, Guidotti S, Camurati I, Frabetti R, Nifant'ev IE, Laishevtsev IP. Macromol Chem Phys, in press.
[34] Covezzi M, Fait A. PCT Int Appl WO 01/44319. Basell, Italy; 2001.
[35] Moraglio G, Gianotti G, Bonicelli U. Eur Polym J 1973;9:693.
[36] (a) Guerra G, Petraccone V, De Rosa C, Corradini P. Makromol Chem Rapid Commun 1985;6:573.
(b) Corradini P, Petraccone V, De Rosa C, Guerra G. Macromolecules 1986;19:2699.
[37] (a) Peterlin A. J Mater Sci 1971;6:490. Peterlin A, Ingram P, Kiho H. Makromol Chem 1965;86:294.
(b) Peterlin A. Kolloid-Z u Z Polym 1967;216:129.
[38] (a) Kobayashi K. In: Geil PH, editor. Polymer single crystals. New York: Interscince; 1963. p. 465.
(b) Matsumoto T, Kawai T, Maeda H. Makromol Chem 1967;107:250.
(c) Petermann J, Kluge W, Gleitner H. J Polym Sci Polym Phys Ed 1979;17:1043.
(d) Krug H, Karbach A, Petermann J. Polymer 1984;25:1687.
[39] (a) Asano T, Fujiwara Y. Polymer 1978;19:99.
(b) Asano T, Fujiwara Y, Yoshida T. Polym J 1979;11:383.
(c) Yoshida T, Fujiwara Y, Asano T. Polymer 1983;24:925.
[40] Mezghani K, Phillips PJ. Polymer 1998;39:3735.
[41] (a) Brückner S, Meille SV. Nature 1989;340:455.
(b) Meille SV, Brückner S, Porzio W. Macromolecules 1990;23:4114.
[42] Ran S, Zong X, Fang D, Hsiao BS, Chu B, Phillips RA. Macromolecules 2001;34:2569.
[43] Treolar LRG. The physics of rubber elasticity. Oxford: Claderon Press; 1975.
[44] Tosaka M, Murakami S, Poompradub S, Kohjiya S, Ikeda Y, Toki S, et al. Macromolecules 2004;37:3299.